Material-efficient preparation and thermoelectric properties of metallic Ni_xAu_{1-x} films with large power factor

A. Riss,[1,*] F. Garmroudi,[1] M. Parzer,[1] C. Eisenmenger-Sittner,[1] A. Pustogow,[1] T. Mori,[2,3] and E. Bauer[1]

[1] *Institute of Solid State Physics, Technische Universität Wien, 1040 Vienna, Austria*
[2] *International Center for Materials Nanoarchitectonics (WPI-MANA), National Institute for Materials Science, Tsukuba 305-0044, Japan*
[3] *University of Tsukuba, Tsukuba 305-8577, Japan*

Thermoelectric materials can utilize the Seebeck effect to convert electrical into thermal energy and vice versa. State-of-the-art thermoelectric materials are semiconductors as the band gap in their electronic density of states results in large values of the Seebeck coefficient. However, recent results suggest that certain metallic alloys such as Ni_xAu_{1-x} can also feature promising thermoelectric properties, relevant for technological applications (Fabians Paper ausgeschrieben zitieren). In this work, we study the thermoelectric potential of NiAu films on different substrates, with additional focus on a cost-efficient synthesis. Ultimately, a large power factor of $11.2\,\mathrm{mW/mK^2}$ is achieved at 614 K in $Ni_{0.27}Au_{0.73}$. Furthermore, by neglecting the phonon contribution to thermal conduction, which is negligibly small in these metallic systems well-obeying the Wiedemann-Franz law, a figure of merit of $zT = 0.15$ is obtained at 763 K.

INTRODUCTION

In times of a rapidly changing climate and increasing global temperature, the necessity of using energy more efficiently and lowering the amount of waste heat is clearly apparent. As of 2012, the vast majority of the global primary energy ($\approx 72,\%$) is lost at conversion, with thermal losses having the largest share, as estimated by Forman *et al.* [1]. Thermoelectric materials have demonstrated to be able to partially convert thermal into electric energy by making use of the Seebeck effect. The efficiency of such a material depends on the figure of merit $zT = S^2\sigma T/\lambda$, where S is the Seebeck coefficient, σ the electrical conductivity and $\lambda = \lambda_{\mathrm{ph}} + \lambda_{\mathrm{el}}$ the thermal conductivity, composed of contributions from phonons and electrons, respectively. All but the phonon thermal conductivity strongly depend on the charge carrier concentration [2], thus preventing the simultaneous optimization of all electronic properties by means of simple aliovalent doping. Instead, more sophisticated strategies, such as band convergence, modulation doping or mobility enhancement are necessary [3]. The electrical conductivity and electron thermal conductivity are further coupled trough the Wiedemann-Franz law $\lambda_{\mathrm{el}}\sigma = LT$ with the Lorenz number L. The phonon thermal conductivity is the only parameter than can be partially manipulated without effecting electronic transport to a significant extent.

In good metals, $\lambda_{\mathrm{el}} \gg \lambda_{\mathrm{ph}}$ and the figure of merit reduces to

$$zT = \frac{S^2}{L} + \mathcal{O}\left(\frac{\lambda_{\mathrm{ph}}}{\lambda_{\mathrm{el}}}\right) . \tag{1}$$

In the metallic limit, the performance thus only depends on the Seebeck coefficient of the material.

Since A. Ioffe's proposal of the superiority of semiconductors over metals [4], thermoelectric research has almost entirely focused on finding, designing and improving systems composed of semiconductors. This is based on the assumption that a finite band gap is necessary to obtain a sufficient asymmetry of the electronic density of states $N(E)$ with respect to the Fermi level. However, the Seebeck coefficient additionally depends on the scattering time τ [5], which can also strongly vary with energy, causing an asymmetry. In a first approximation, the Seebeck coefficient can be determined from the well-known Mott formula

$$S = -\frac{\pi^2 k_{\mathrm{B}}^2}{3e} T \left(\frac{\partial \ln N}{\partial E} - \frac{\partial \ln \tau^{-1}}{\partial E} \right)_{E_{\mathrm{F}}} . \tag{2}$$

Garmroudi *et al.* combined experimental data and theoretical calculations of Ni_xAu_{1-x} alloys to demonstrate that the Seebeck coefficient is significantly increased in transition metals when the Fermi energy closely aligns with the d states [6].

The presence of flat d bandes in Ni results in a considerable $\partial \ln N/\partial E$, but their lower conductivity diminishes their overall contribution to the total Seebeck coefficient, as described by the formula

$$S = \frac{S_s\sigma_s + S_d\sigma_d}{\sigma_s + \sigma_d} , \tag{3}$$

where s and d denote the s and d states, respectively. Consequently, the dominant contribution to S primarily originates from the highly mobile and more conductive s states.

In the context of the Mott formula, the first term in Equation 2 is neglectable in s and p states due to their broad bandwidth. Conversely, in the case of Au s sates scattering into Ni d states, there is a significant increase in the scattering rate τ^{-1} within the energy range of Ni d states. This results in a substantial enhancement of the second term in Equation 2, $\partial \ln \tau^{-1}/\partial E$. By partially substituting Ni with Au, effectively shifting the Fermi energy closer to the edge of the d band, Garmroudi *et al.*

achieved a remarkable increase in the power factor, reaching 34 mW/mK^2 in $Ni_{0.1}Au_{0.9}$ at 560 K [6].

In this study, we attempt to replicate the crystal structure and thermoelectric properties of the bulk in films deposited on various substrates. We place particular emphasis on developing a cost-effective synthesize method, addressing the challenge associated with the costly preparation of Au-rich bulk materials.

EXPERIMENTAL DETAILS

The sputter target was prepared from a Ni disk with a diameter of 25.4 mm, onto which either two or three flattened Au pieces were affixed through spot-welding. Once in place, the target was compressed with a pressure of 200 bar. This not only led to great electrical and thermal contacts but also ensured a decent mechanical connection, although strong vibrations could potentially dislodge the Au components. Each Au piece weighted approximately 0.5 g and a single target could produce between 20 to 30 films (depending on the desired thickness), which highlights the cost-efficiency of the approach.

It's worth noting that the overall target thickness is restricted to < 1.5 mm due to the ferromagnetic behavior of Ni. Otherwise, the target could disrupt the magnetic field within the sputter chamber by causing a short-circuiting of the field. Consequently, the thickness has a significant impact on the required gas pressure for initiating the gas discharge.

The sputtering process was conducted at a temperature of 500 °C utilizing direct-current (DC) magnetron sputtering, with a power of either 5 W or 10 W, a target-substrate distance of 30 mm and a working gas pressure of 0.05 mbar. Prior to the deposition, the substrates were cleaned with acetone and ethanol. The substrates encompassed unpolished Si and yttria-stabilized zirconia (YSZ) as well as polished quartz glass.

The films' composition was characterized using energy-dispersive X-ray (EDX) spectroscopy, conducted with the FEI Quanta 250 FEG. The crystal structure was determined using the X'Pert MPDII diffractometer from Panalytical in the Bragg-Brentano geometry. To minimize reflection peaks from the single-crystalline substrates, an offset of $\omega = 3°$ was applied. For electrical resistivity and Seebeck coefficient measurements, the ZEM-3 equipment from ULVAC was used.

RESULTS

Composition and crystal structure

The composition of all samples is depicted in Figure 1a. The x-axis shows the sample number in chronological sequence, effectively representing the progression of the target ablation. It is evident that the amount of Ni increases as more material is removed from the target. This phenomenon is likely attributed to the finite surface area and volume of the Au pieces in contrast to the quasi-infinite Ni layer beneath. Films originating from the target with less Au exhibited an average Ni content of $x = 0.56$, roughly twice the amount found in films deposited from the Au-rich target ($x = 0.24$ on average). It is essen-

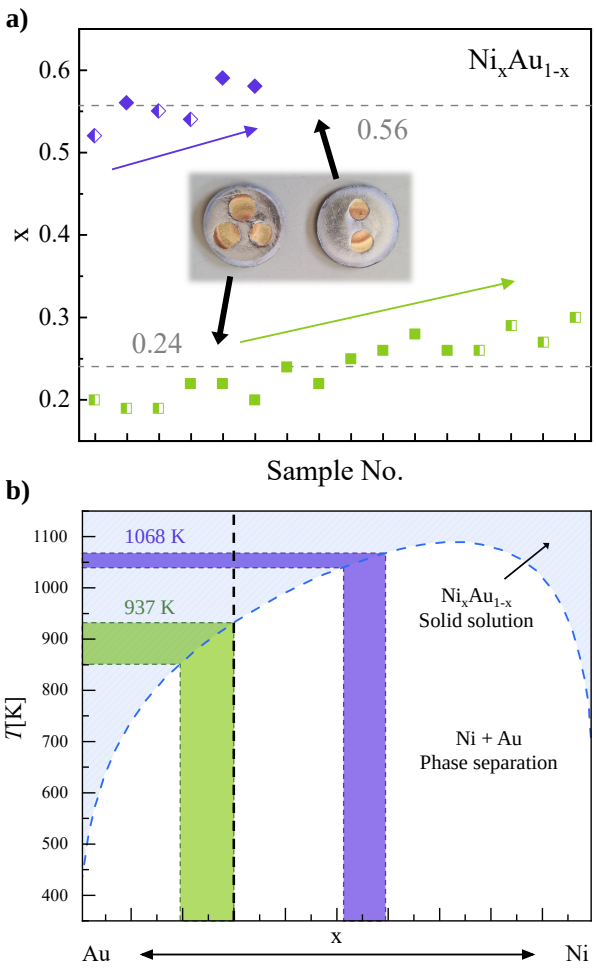

Figure 1: a) Composition of all films versus the sample number. The purple and green points belong to films sputtered from the target with two and three Au pieces shown in the inset, respectively. Half-filled symbols indicate films made at a power of 5 W, while filled symbols represent films made at 10 W. The gray dashed lines highlight the mean amount of Ni in the films. b) Phase diagram of binary Ni-Au [7]. The blue area marks the region of solubility. The purple and green areas highlight the necessary annealing temperature to obtain a single phase. For $x < 0.3$, perfect solubility was found without quenching, as illustrated by the black dashed line [6].

tial to highlight that precise control over the composition through the strategic placement of Au is challenging due to several uncertainties, *e.g.* the precise positioning relative to the magnetron-sputtering ablation ring and the size, shape and even thickness of the Au pieces, which can manipulate the ion current distribution on the target. Instead, achieving the desired composition necessitates adjustments to parameters like working gas pressure, target-substrate distance and offset and power, all of which are known to impact the film's composition [8–11]. For example, examining the purple data points in Figure 1a reveals that the amount of Ni is slightly higher at 10 W compared to 5 W. It is important to note that the conventional theory, which posits that the ratio of ejected atoms equals the target's composition due to surface adjustments, does not apply in this context. This is because the two elements are spatially separated and not intermixed, making the individual energy-dependent sputtering yields a critical factor to consider [8].

The phase diagram of binary Ni – Au alloys is presented in Figure 1b [7]. In the blue-shaded region, the elements exhibit complete solubility, forming a solid solution. At lower temperatures, they tend to segregate, leading to the formation of Ni-rich and Au-rich phases. To obtain single-phase films, it is necessary to sputter or anneal at specific temperatures, with upper limits of 937 K and 1068 K for films produced from targets with 3 and 2 Au components, respectively. Garmroudi *et al.* achieved stabilization of the solid solution in bulk materials at room temperature by rapidly quenching the samples in water, effectively preserving the metastable crystal structure [6]. However, it's worth noting that for $x < 0.3$ the authors observed that a single phase could also be obtained through gradual furnace cooling, as indicated by the black dashed line in Figure 1b.

Figure 2a-c shows the diffraction pattern of films on quartz glass, Si and YSZ before and after annealing at 600 °C for three days. Prior to annealing, the films deposited on glass, with a composition of $Ni_{0.58}Au_{0.42}$, exhibit a phase resembling $Ni_{0.6}Au_{0.4}$ with minor traces of pure Au (see Figure 2a). Upon annealing, the structure undergoes a transformation, shifting towards an Au-rich $Ni_{0.12}Au_{0.88}$ phase along with pure Ni. This transformation aligns with findings from bulk alloy measurements [6].

On Si substrates (Figure 2b), the same $Ni_{0.6}Au_{0.4}$ phase is formed within the $Ni_{0.52}Au_{0.48}$ sample, while the Au-rich film predominantly comprised $Ni_{0.2}Au_{0.8}$ despite a subtle presence of a Ni-rich peak. This agrees with the alloy's stability predicted for $x < 0.3$. Subsequent to the annealing process, an almost pure Au phase ($Ni_{0.03}Au_{0.97}$ forms irrespective of the initial composition. Any remaining Ni disperses from the primary phase, manifesting as $NiSi_2$. Notably, the crystal structure exhibits only slight variations between the samples with $x = 0.22$ and $x = 0.52$, primarily reflecting differences in the $NiSi_2$ content. The Au-rich sample additionally comprised tiny amounts of a CuAu phase, which could originate from the copper plate of the sputtering chamber.

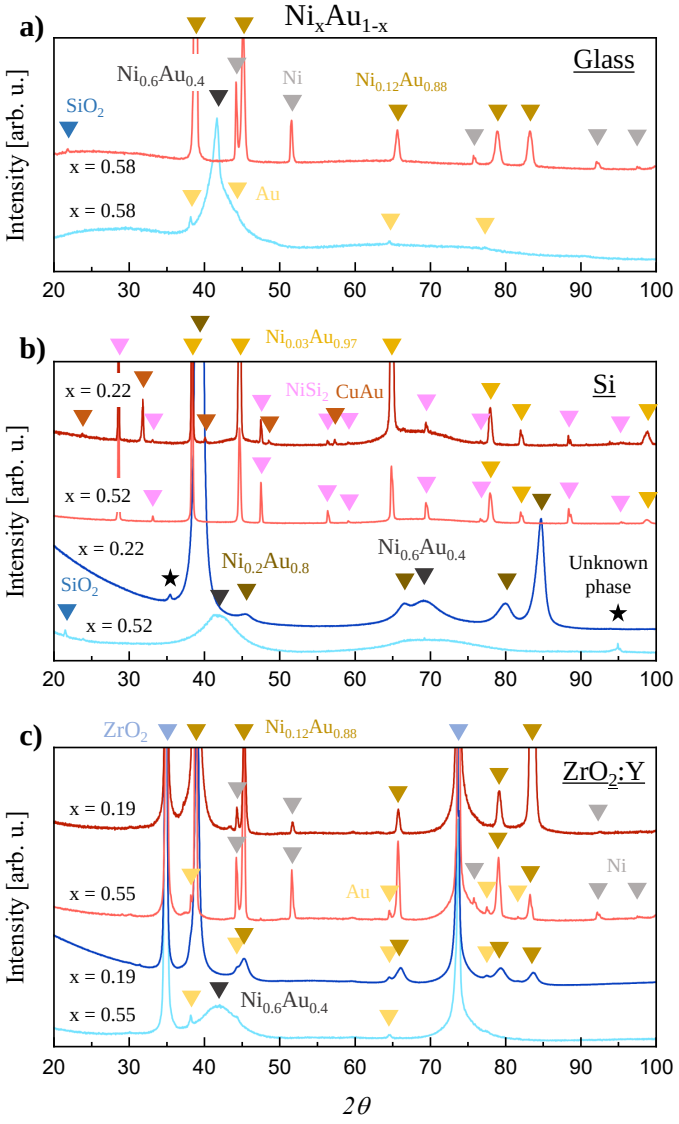

Figure 2: X-ray diffraction pattern of NiAu films on a) polished quartz glass, b) unpolished Si and c) unpolished YSZ. In each case, the blue and red lines represent samples before and after annealing at 600 °C for three days, respectively. The Ni content, denoted as x, is displayed on the left side of each line for reference.

The films deposited on YSZ with a composition of $Ni_{0.55}Au_{0.45}$ show a tendency similar to that observed in the samples on quartz glass, as depiced in Figure 2c. Without annealing, these films adopt a $Ni_{0.6}Au_{0.4}$ phase together with pure Au. Upon annealing, this phase disperses into $Ni_{0.12}Au_{0.88}$ along with the emergence of pure Ni. Much like the films on Si, the same crystal structure is observed on YSZ after annealing, irrespective of the

composition. However, in the case of Au-rich films, the reduced Ni content leads to a decrease in the presence of pure Ni.

In summary, no significant difference in the crystal structure is observed among the three substrates concerning the Ni_xAu_{1-x} phase. On Si, however, $NiSi_2$ forms, while in the other two substrates, pure Ni persists. Prior to annealing, most samples contain minor traces of pure Au, hinting at a potential lack of thermal energy to stabilize into the favourable crystal structure. This is likely attributed to the sputtering setup where the heater is positioned within a copper plate beneath the substrate. The weak thermal contact between the copper and the substrate causes a decrease of the temperature which is exacerbated by the low thermal conductivity of glass ($\lambda \approx 1\,\mathrm{W/mK}$) and YSZ ($\lambda \approx 2\,\mathrm{W/mK}$) [12, 13]. Conversely, on Si, the temperature is expected to be several degrees higher due to the significantly larger thermal conductivity ($\lambda \approx 150\,\mathrm{W/mK}$) [14] and the thinner substrate (280 µm compared to 560 µm of YSZ and 1 mm of glass). These circumstance facilitates the formation of the desired crystal structure.

Thermoelectric properties

Considering that pure Ni and Au exhibit Seebeck coefficients of only $\approx -10\,\mu\mathrm{V/K}$ and $\approx 3\,\mu\mathrm{V/K}$ above room temperature, respectively, and given that multiple, non-interacting phases tend to have a detrimental effect on the overall material properties [composite paper zitieren], it is reasonabel to expect that films exhibiting multiple phases would yield a lower performance compared to the bulk material with the same NiAu phase.

The measured thermoelectric properties, along with the estimated figure of merit zT derived from Equation 1, are illustrated in Figure 3. For comparative purposes, the data of bulk $Ni_{0.2}Au_{0.8}$ and $Ni_{0.6}Au_{0.4}$ alloys are included, representing compositions that closely resemble those of the films.

Due to the exceedingly low electrical resistivity of NiAu alloys, a contribution of any of the substrates can be ruled out at room temperature. However, at elevated temperatures, the substantial decrease in electrical resistivity in Si results in a modification of the measured Seebeck coefficient and electrical resistivity of the film-substrate system, leading to non-physical values above 550 K [15].

The Seebeck coefficient does not exhibit a significant dependence on the substrate, as corroborated by the X-ray diffraction pattern. An exception to this trend is observed in annealed films on the Si substrate, where a considerable reduction in thermopower is evident. This decline is presumably a consequence of Si diffusion and the substantial formation of a $NiSi_2$ phase.

Films deposited from the target with less Au uniformly exhibit the $Ni_{0.6}Au_{0.4}$ phase prior to annealing (indicated by the light blue lines) and closely align with the respective bulk properties. Although the resistivity is higher due to limited ordering, the Seebeck coefficient, and consequently zT, show a slight improvement. This enhancement is attributed to the decomposition of the bulk for $x \geq 0.3$, a phenomenon observed only in the films after annealing. In the case of Au-rich films on Si, a $Ni_{0.2}Au_{0.8}$ phase forms upon sputtering, in contrast to films on YSZ, where a $Ni_{0.12}Au_{0.88}$ phase coexists with pure Au. Consequently, the film on Si exhibits a Seebeck coefficient closer to the respective bulk value, albeit substantially reduced. Ultimately, on Si, the power factor and figure of merit reach $PF = 6.7\,\mathrm{mW/mK^2}$ in $Ni_{0.22}Au_{0.78}$ at 418 K and $zT = 0.1$ $Ni_{0.52}Au_{0.48}$ at 344 K.

Annealed films deposited on Si manifest a Au-dominant $Ni_{0.03}Au_{0.97}$ phase alongside $NiSi_2$, causing a detrimental effect on the Seebeck coefficient and, consequently, overall thermoelectric performance. Thus, the interaction of Ni with Si renders Si substrates unsuitable for the deposition of NiAu alloys.

The comparable diffraction pattern observed in films deposited on glass ($Ni_{0.58}Au_{0.42}$) and YSZ ($Ni_{0.55}Au_{0.45}$), both forming $Ni_{0.12}Au_{0.88}$ upon annealing, is also pronounced by closely aligned thermoelectric properties. Nonetheless, the performance is below that of bulk $Ni_{0.2}Au_{0.8}$ and $Ni_{0.1}Au_{0.9}$ ($PF \approx 20 - 30\,\mathrm{mW/mK^2}$ around room temperature [6]). The Seebeck coefficient is notably increased in Au-rich films on YSZ despite the similar crystal structure. However, the reduced Ni content mitigates the adverse effect of multi-phase contributions. Ultimately, $PF = 11.2\,\mathrm{mW/mK^2}$ at 614 K and $zT = 0.15$ at 763 K in $Ni_{0.19}Au_{0.81}$ deposited on YSZ.

Adopting the method suggested by Garmroudi *et al.* [6], an attempt was made to achieve a single phase by annealing samples in an Ar-filled quartz tube at 937 K and 1068 K, followed by rapid quenching in water. Unfortunately, this approach proved challenging as the thermal shock caused the substrates to fracture. Further experiments involving rapid cooling in air also proved unsuccessful and had a detrimental effect on the thermoelectric properties of the materials. Thus, future work should focus on using different substrates with better mechanical properties to withstand the thermal shock during water quenching.

CONCLUSION

Ni_xAu_{1-x} films have been successfully prepared via DC magnetron sputtering, employing a single Ni target to with Au pieces were affixed. The Au components had a combined weight ranging from 1 to 2 g, allowing for the production of 20 to 30 films per target, demonstrating the cost-effectiveness of this single-target approach.

Achieving precise control over the composition proved to be challenging due to various uncertainties, including

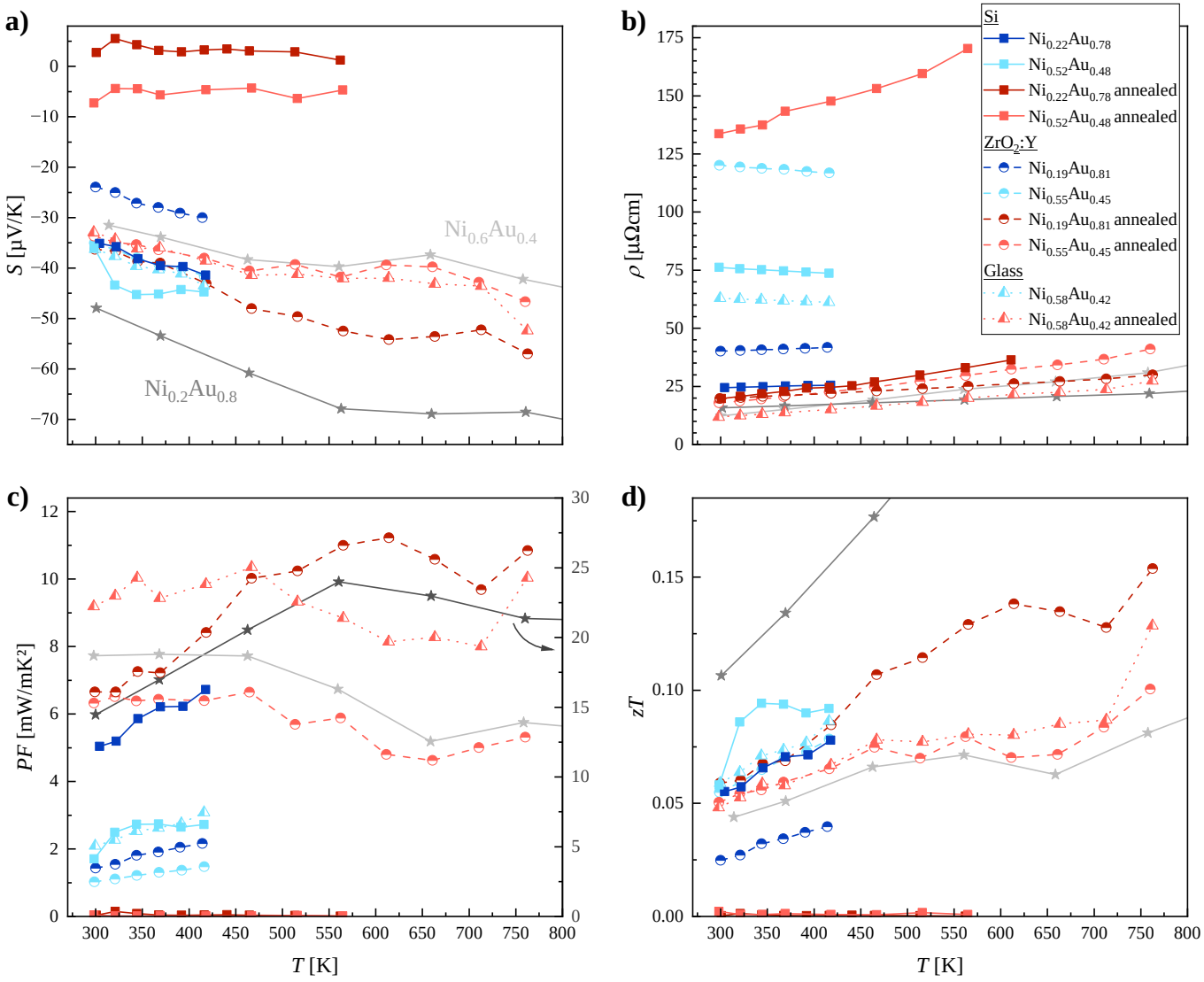

Figure 3: a) Seebeck coefficient, b) electrical resistivity, c) power factor and d) figure of merit of films deposited on Si, YSZ and glass substrates. Blue and red data points correspond to samples before and after annealing, respectively. The gray lines show bulk properties of $Ni_{0.1}Au_{0.9}$ and $Ni_{0.6}Au_{0.4}$ for comparison, taken from Ref. [6].

the positioning of Au pieces relative to the magnetron-sputtering ablation ring and the shapes of the pieces. Additionally, the thickness of the Ni layer influenced the magnetic field and, consequently, the ion current onto the target surface. To manipulate the composition effectively, other sputtering-related parameters, such as working gas pressure, power and substrate-target distance and offset, have to be tuned.

After deposition, the films exhibited phases close to stoichiometry, though the limited degree of ordering and traces of secondary phases hampered overall performance. Upon annealing, the phases transformed, shifting towards Au-rich phases and pure Ni. The thermoelectric properties depend on the amount of pure Ni or related phases, such as $NiSi_2$. Ultimately, a power factor of 11.2 mW/mK^2 and figure of merit of 0.15 was achieved in $Ni_{0.19}Au_{0.81}$ deposited on YSZ.

To optimize the performance of NiAu films, rapid quenching in water appears necessary. However, the challenge lies in finding a suitable setup or substrate to prevent film failure during this process.

ACKNOWLEDGEMENTS

Financial support for the research in this paper was granted by the Japan Science and Technology Agency (JST) programs MIRAI, JPMJMI19A1. We acknowledge the X-ray Center at TU Wien for providing their equipment. Furthermore, USTEM at TU Wien is acknowl-

edged for providing the scanning electron microscope to study the composition of NiAu films.

* alexander.riss@tuwien.ac.at

[1] C. Forman, I. K. Muritala, R. Pardemann, and B. Meyer, Renewable and Sustainable Energy Reviews **57**, 1568 (2016).
[2] G. J. Snyder and E. S. Toberer, Nature materials **7**, 105 (2008).
[3] G. Tan, L.-D. Zhao, and M. G. Kanatzidis, Chemical reviews **116**, 12123 (2016).
[4] A. Ioffe, The socialist reconstruction and science **1**, 23 (1932).
[5] A. Zevalkink, D. M. Smiadak, J. L. Blackburn, A. J. Ferguson, M. L. Chabinyc, O. Delaire, J. Wang, K. Kovnir, J. Martin, L. T. Schelhas, *et al.*, Applied Physics Reviews **5** (2018).
[6] F. Garmroudi, M. Parzer, A. Riss, C. Bourgès, S. Khmelevskyi, T. Mori, E. Bauer, and A. Pustogow, arXiv preprint arXiv:2303.03062 (2023).
[7] J. Wang, X.-G. Lu, B. Sundman, and X. Su, Calphad **29**, 263 (2005).
[8] N. Matsunami, Y. Yamamura, Y. Itikawa, N. Itoh, Y. Kazumata, S. Miyagawa, K. Morita, R. Shimizu, and H. Tawara, Atomic data and nuclear data tables **31**, 1 (1984).
[9] A. Rogov and Y. V. Kapustin, Instruments and Experimental Techniques **63**, 776 (2020).
[10] E. Särhammar, E. Strandberg, J. Sundberg, H. Nyberg, T. Kubart, S. Jacobson, U. Jansson, and T. Nyberg, Surface and Coatings Technology **252**, 186 (2014).
[11] J. Neidhardt, S. Mráz, J. M. Schneider, E. Strub, W. Bohne, B. Liedke, W. Möller, and C. Mitterer, Journal of applied physics **104** (2008).
[12] C. Kittel, Physical Review **75**, 972 (1949).
[13] J.-F. Bisson, D. Fournier, M. Poulain, O. Lavigne, and R. Mévrel, Journal of the American Ceramic Society **83**, 1993 (2000).
[14] H. Shanks, P. Maycock, P. Sidles, and G. Danielson, Physical Review **130**, 1743 (1963).
[15] A. Riss, M. Stöger, M. Parzer, F. Garmroudi, N. Reumann, B. Hinterleitner, T. Mori, and E. Bauer, Physical Review Applied **19**, 054024 (2023).